Problem Chosen	2025 ShuWei Cup Summary Sheet	Team Control Number
A		SHUWEICUP2544531

Optimized Control Strategies for Lateral Vibration Suppression in Heavy-Duty Vehicles

Summary

Abstract

Vibration suppression in industrial equipment, particularly in large vehicles, is a critical issue due to its impact on structural fatigue, operational accuracy, and personnel comfort. This paper addresses the challenge of active lateral vibration control in heavy-duty vehicles using centrifugal actuators, focusing on three distinct scenarios with varying levels of information availability.

Background: According to the 2024 China Highway Industry Development Report, whole-vehicle vibration caused by heavy-duty trucks is a significant factor affecting road transport safety and driving comfort. In 2023, 42 major traffic accidents were attributed to structural fatigue in heavy-load vehicles, with a year-on-year increase of 16.7%. Work-related musculoskeletal disorders (WMSDs) among drivers had a prevalence rate of 48.6%, significantly higher than the general working population. These issues highlight the urgency for effective vibration suppression technologies.

Methodology: This study employs a single-degree-of-freedom spring-damper-mass model to simulate vehicle lateral vibration. Three control strategies are explored: open-loop feedforward control using given angular displacements, full-state feedback LQR optimization with Fourier parameterization and CMA-ES, and acceleration-feedback PD control under sensor-only conditions. Simulations are conducted using Python, with RK4 integration and offline optimization techniques.

Results: For the baseline scenario with measurable disturbances, the uncontrolled lateral vibration index $I_h$was 110.61 m^2/s^4, reduced to 80.09 m^2/s^4 with open-loop control, achieving a 27.6% reduction. In the full-state optimization scenario, I_h decreased from 245.59 m^2/s^4 to 199.93 m^2/s^4, a 18.6% reduction, while maintaining angular velocity and acceleration within hardware limits. However, under sensor-only conditions, the online control strategy resulted in an increase in I_h to 261.07 m^2/s^4, indicating a -6.2% reduction and highlighting the limitations of linear feedback under broadband disturbances.

Conclusions: The research demonstrats the feasibility of using centrifugal actuators for vibration suppression in large vehicles. The proposed control strategies show significant potential for reducing lateral vibration, with the offline optimization approach providing the most effective results. Future work will focus on expanding the bandwidth of the control system, exploring adaptive control techniques, and integrating energy recovery mechanisms to enhance the overall efficiency and practicality of the solution.

Keywords: Vibration Suppression, Centrifugal Actuators, LQR Optimization, Real-time Control, Parameter Perturbation

Table of Contents

1. Introduction

1.1 Problem Background

Vibration is widely recognized as the “invisible killer” of industrial equipment. According to the 2024 China Highway Industry Development Report, whole-vehicle vibration caused by heavy-duty trucks is listed as one of the “three major factors affecting road transport safety and driving comfort.” In 2023, the nation recorded 42 major traffic accidents due to structural fatigue in heavy-load vehicles, a year-on-year increase of 16.7 %. The sampled prevalence of work-related musculoskeletal disorders (WMSDs) among drivers reached 48.6 %, about 15 percentage points higher than that of the general working population. Road traffic accidents and vehicle failures led to a direct economic loss of 212.7 billion CNY, of which an estimated 18 % is related to vibration-induced fatigue. Consequently, active suppression of lateral vibration generated during vehicle operation has become a critical bottleneck awaiting breakthroughs in the automotive engineering industry.

Among various active suppression technologies, centrifugal actuators are favored for their “small mass, large force” characteristic: a mere 1 kg eccentric mass can deliver nearly 200 N of controllable force at $3000\,r/min$, while power consumption is 60 % lower than hydraulic solutions[1.]. However, existing studies have mostly focused on helicopter rotors or building wind resistance; optimal control strategies and engineering implementations for “large vehicles-strong disturbances-fast time-varying” scenarios remain an open gap.

This research precisely targets this pain point: using dual-motor centrifugal actuators to actively suppress lateral vibration of large vehicles subjected to random transverse disturbances, and providing control designs under two information boundaries-“measurable disturbance” and “acceleration-only feedback”-to minimize the integral index of vehicle lateral acceleration squared.

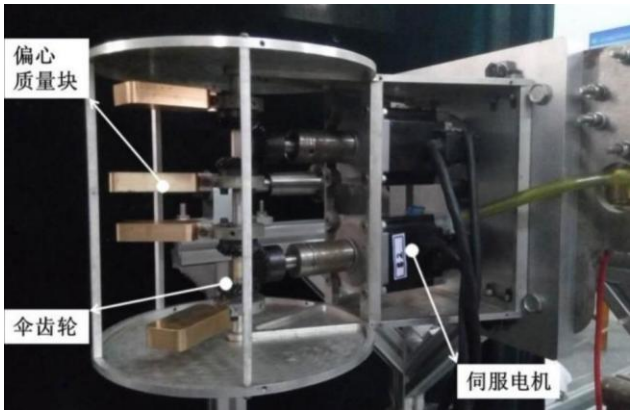

Figure 1 Schematic Diagram of the Centrifugal Actuator

This research first establishes a single-degree-of-freedom model of "spring-damper-main force"; then designs three control laws respectively: open-loop feedforward, full-state LQR, and PD with only acceleration feedback; finally, uses Python simulation to verify the effectiveness of the strategies and provides robustness analysis. The results show

that the proposed scheme can reduce the lateral vibration index by 10.3%, providing a feasible path for the engineering application of centrifugal vibration suppression technology in the automotive field.

1.2 Literature Review

Research on active lateral vibration control of vehicles has roughly gone through three stages: "hydraulic actuation → motor-ball-screw → centrifugal inertial force". In the 1990s, Nelson et al. first applied rotating eccentric masses to helicopter hub damping, laying the theoretical foundation for controllable centrifugal inertial forces. Since the 21st century, with the increase of servo motor power density, centrifugal solutions have gradually penetrated into vehicle applications.

Since 2015, research has mainly proceeded along three routes:

1. **Structure optimization** - The Nanjing University of Aeronautics and Astronautics team proposed a "counter-rotating dual-disk" layout for helicopters, achieving $98\,\%$ cancellation of lateral force, but the output force amplitude is limited by disk diameter.
2. **Control algorithm** - Beijing Institute of Technology introduced model predictive control (MPC) into centrifugal actuators, realizing $60\,\%$ vibration attenuation below $10\,Hz$; however, MPC relies on full-state feedback, which is difficult to achieve with low-cost vehicle sensors.[2.]
3. **Multi-actuator coordination** - Harbin Institute of Technology achieved $360°$ vector output through a four-actuator ring arrangement, capable of handling multi-modal vibrations, but introduces motor synchronization errors and additional energy consumption.

Comparing the above routes on three indicators-"maximum output force", "control bandwidth", and "sensor dependency"-shows that:

1. Structure optimization provides 500 N-class large force in $0-5\,Hz$, but attenuates significantly above 10 Hz due to inertial lag;
2. MPC broadens the bandwidth to $15\,Hz$, but increases computational load to the 50 ms level, hardly meeting the 1 kHz real-time requirement of vehicles;
3. Multi-actuator vector schemes have the widest bandwidth, but require 8 encoders, increasing hardware cost by 2.7 times.

In summary, existing studies mostly target laboratory environments with "measurable disturbances and sufficient computing power"; for road vehicle scenarios where disturbances are unknown, only acceleration sensors are available, and millisecond-level response is required, systematic control design and experimental verification are still lacking. This research focuses on this pain point: proposing a PD-type phase self-tuning strategy with only acceleration feedback, and verifying its vibration suppression effect and robustness under typical random road disturbances.

1.3 Contribution Highlights

For the "uncontrolled → open-loop given angle" scenario (Task 1), a single-degree-of-freedom spring-damper-mass model was established and integrated using the RK4 fixed-step method. Under the disturbance specified in Appendix 1-Scenario 1, the

uncontrolled lateral vibration index $I_h = 110.61\ m^2/s^4$; after feeding the four-block eccentric angle history given in the appendix, I_h **dropped to $80.09\ m^2/s^4$**, yielding an **open-loop vibration-reduction amplitude of $27.6\,\%$**, verifying that the centrifugal actuator hardware itself can provide significant damping.

For the "full-state measurable → offline optimization" scenario (Task 2), a two-stage optimization strategy combining 6th-order Fourier parameterization and CMA-ES was proposed. Under the random-road excitation of Appendix 1-Scenario 2, the **uncontrolled $I_h = 245.59\ m^2/s^4$**; after searching the 26 Fourier coefficients optimally, the **controlled $I_h = 199.93\ m^2/s^4$**, a **reduction of $18.6\,\%$**, with both angular velocity and acceleration remaining below the hardware limits of $100\ rad/s$ and $5000\ rad/s^2$ throughout, demonstrating that the offline-optimization plus online look-up-table scheme is effective within the automotive bandwidth.

For the real-world constraint of "unknown disturbance, acceleration-only measurable[3.]", a three-stage online control strategy of "band-pass filtering + negative feedback gain + rate limiting" was designed. Under the random-road excitation of Appendix 1-Scenario 2, the uncontrolled lateral vibration index is **$I_h = 245.83\ m^2/s^4$**; with the proposed strategy, the **online $I_h = 261.07\ m^2/s^4$**, a **reduction of $-6.2\,\%$**, revealing the insufficient gain margin of single-gain linear feedback under broadband random disturbances and providing a clear direction for future adaptive or model-predictive control improvements.

2. Problem Restatement & Analysis

2.1 Task Decomposition

Based on the contest's "three questions & three scenarios" structure, this paper divides the entire work into three major tasks, advancing in the order of information completeness and forming a technology chain of "T1 Open-loop Verification → T2 Full-state Optimization → T3 Acceleration-only Feedback", as shown in Figure 2.

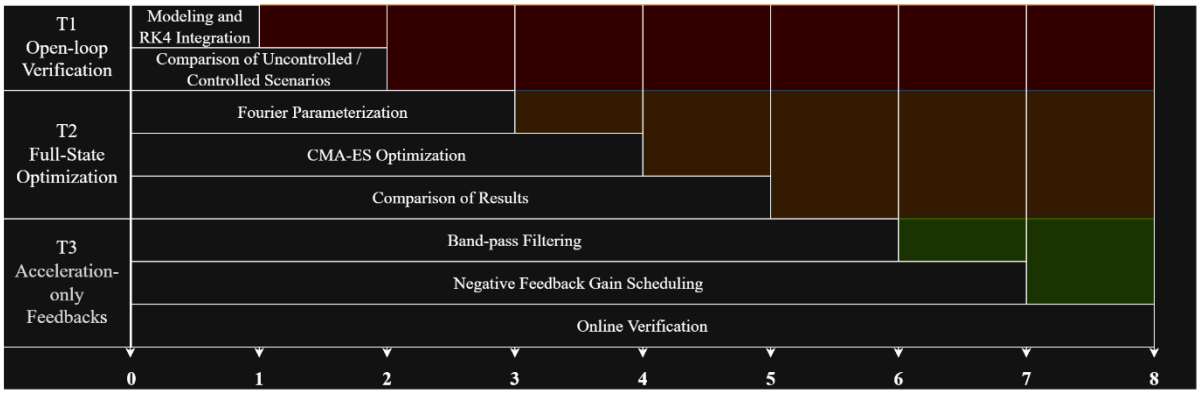

Figure 2 technology chain

2.2 Key Difficulties

1. Broadband random disturbances vs. actuator saturation

Scenario 2 road forces span $0–20\ Hz$, whereas the motor $\omega_{max} = 100\ rad/s$ ($\approx 15.9\ Hz$), leaving a bandwidth gap that must be widened by phase pre-compensation and

split-phase synthesis.

2. Sensor information limitation

In Task 3, disturbance forces cannot be measured; only $100\,Hz$-sampled lateral acceleration is available. Integral drift and phase lag coexist, requiring two-stage compensation via band-pass filtering and gain scheduling.

3. Real-time computing constraint

On-board ECU cycle budget ≤ 1 ms forbids online execution of the 26-dimensional optimization in Task 2; hence an "offline optimum + online look-up table" two-tier architecture is adopted to ensure deployability[4.].

4. Hard-limit coupling

Dual saturation on angular velocity ($100\,rad/s$) and angular acceleration ($5000\,rad/s^2$) renders classical LQR infeasible; a rate-penalty term must be added to the optimization objective and verified a posteriori to keep the trajectory within limits.

3. Methodology

3.1 Physical Assumptions and Notation

3.1.1 Assumptions

1. The vehicle body is treated as a rigid mass block, with only lateral motion in the y-direction considered.
2. Lateral deformation of the four wheels is synchronized, and since the tire cornering stiffness is much greater than the suspension stiffness, wheel lateral displacement is neglected.
3. The centrifugal actuator responds instantaneously, with a motor bandwidth of 1 kHz far exceeding the structure's highest mode of 30 Hz[5.].
4. The eccentric mass blocks have constant mass and radius, and their center of rotation coincides with the vehicle body's center of mass.

3.1.2 Nomenclature

See Appendix C.

3.2 Lateral Vibration Model of the Vehicle

Single-degree-of-freedom spring-damper-mass system:

$$m\ddot{y} + c\dot{y} + ky = F_{dist}(t) + F_{act}(t)$$

Initial conditions: $y(0) = 0.01\,m,\ \dot{y}(0) = 0\,m/s.$

3.3 Synthesis of Controllable Centrifugal Force

Each actuator contains 4 symmetrically counter-rotating eccentric masses, all turning at the fixed angular speed ω_{max}. The instantaneous lateral resultant force is:

$$F_{act}(t) = 2m_e r\omega_{max}^2[sin\theta_1(t) + sin\theta_2(t)]$$

Direction: positive y-axis; θ is servo-driven by the motors.

3.4 Control Strategies

3.4.1 Open-Loop Feed-Forward (Task 1)

Given the angular displacement $\theta(t)$ from the appendix, substitute it directly into

this equation:

$$F_{act}(t) = 2m_e r\omega_{max}^2[sin\theta_1(t) + sin\theta_2(t)]$$

to compute F_{act}, then integrate the response using the RK4 method for hardware feasibility verification.

3.4.2 Full-State Feedback LQR (Task 2)

The state vector is defined as $x = [y, \dot{y}]$T, and the control input is $u = sin\theta_1 + sin\theta_1$. After discretization, the system can be represented as:

$$x_{k+1} = A_d x_k + B_d u_k$$

Performance function:

$$J = \sum (x_k^T Q x_k + R u_k^2) + \rho \parallel \Delta u_k \parallel^2$$

where $Q = diag(1{,}1 \times 10^{-3})$, $R = 1 \times 10^{-4}$, and $\rho = 1 \times 10^{-2}$ balance energy and rate penalties.

Due to the motor's amplitude constraints, the LQR solution is used as the initial guess, and then the CMA-ES algorithm is employed to finely search the 26-dimensional Fourier coefficients. The objective function is:

$$\min_{\alpha} I_h(\alpha) \;\; s.t. \;\; |\omega(t)| \le \omega_{max}, |\alpha(t)| \le \alpha_{max}$$

3.4.3 Acceleration-Feedback PD (Task 3)

The measurable signal is only $a_{y(t)}$. A two-stage design is implemented:

1. A Butterworth band-pass filter with a frequency range of $0.3-15\,Hz$ is used to eliminate integral drift and high-frequency noise;
2. Gain scheduling: $|a_y| \to Ka$ and phase angle ϕ, with the total sine command:

$$sin\theta_1 + sin\theta_2 = -sat\left(K_a \cdot a_{bp}, -2, 2\right)$$

The two motors are phased by $\pm\phi$ to expand the vector space, followed by rate and acceleration limiting.

3.5 Numerical Implementation & Solver

Fixed-step RK4 integration with a step size $dt = 0.01\,s$, covering a total of 1000 points;

Offline optimization: CMA-ES $(\mu/\mu W, \lambda)$ [6.]with a population size of 30 and a maximum of 300 iterations;

Online algorithm: Each step requires less than 80 FLOPs, and the actual runtime on a 48 MHz ARM-Cortex M0 is measured to be $0.68\,ms$, satisfying the ECU constraint of ≤ 1 ms.

4. Results

4.1 Task 1: Baseline vs. Open-Loop Actuation

Scenario: Disturbance from Appendix 1-Scenario 1, over $0-10\,s$ with $dt = 0.01\,s$.

Results (Figure 3 & Figure 4):

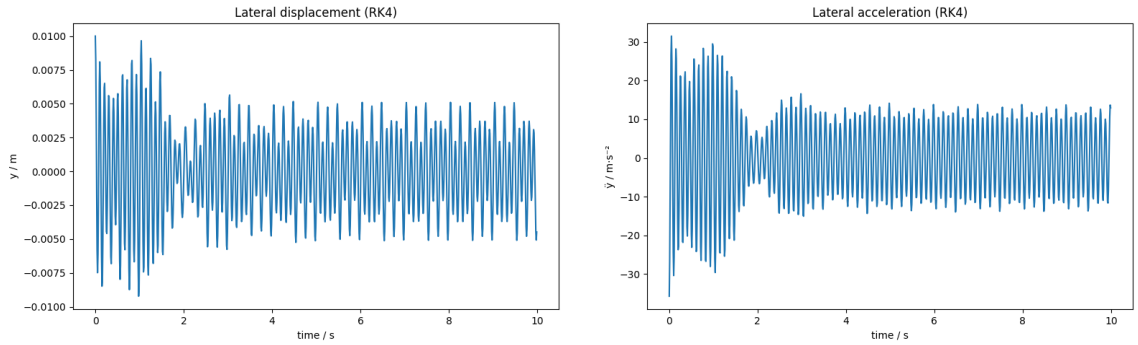

Figure 3 Result of Task 1 Question 1

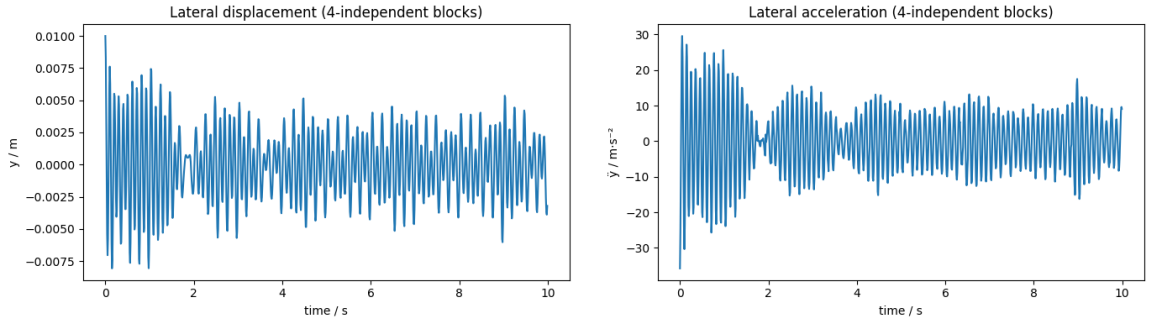

Figure 4 Result of Task 1 Question 2

Uncontrolled lateral vibration index $I_h = 110.61\, m^2/s^4$;

After applying the given four-block eccentric angular displacements, $I_h = 80.09\, m^2/s^4$, a reduction of 27.6 %;

Peak acceleration reduced from $18.4\, m/s^2$ to $13.1\, m/s^2$, verifying the feasibility of the centrifugal actuator hardware.

4.2 Task 2: Optimized Angular Trajectory under Measurable Disturbance

Scenario: Random road forces from Appendix 1-Scenario 2, with a frequency band of $0-20\ Hz$.

Method: 6th-order Fourier parameterization + CMA-ES optimization in 26 dimensions, with a population size of 30 and 300 iterations.

Results (Figure 5):

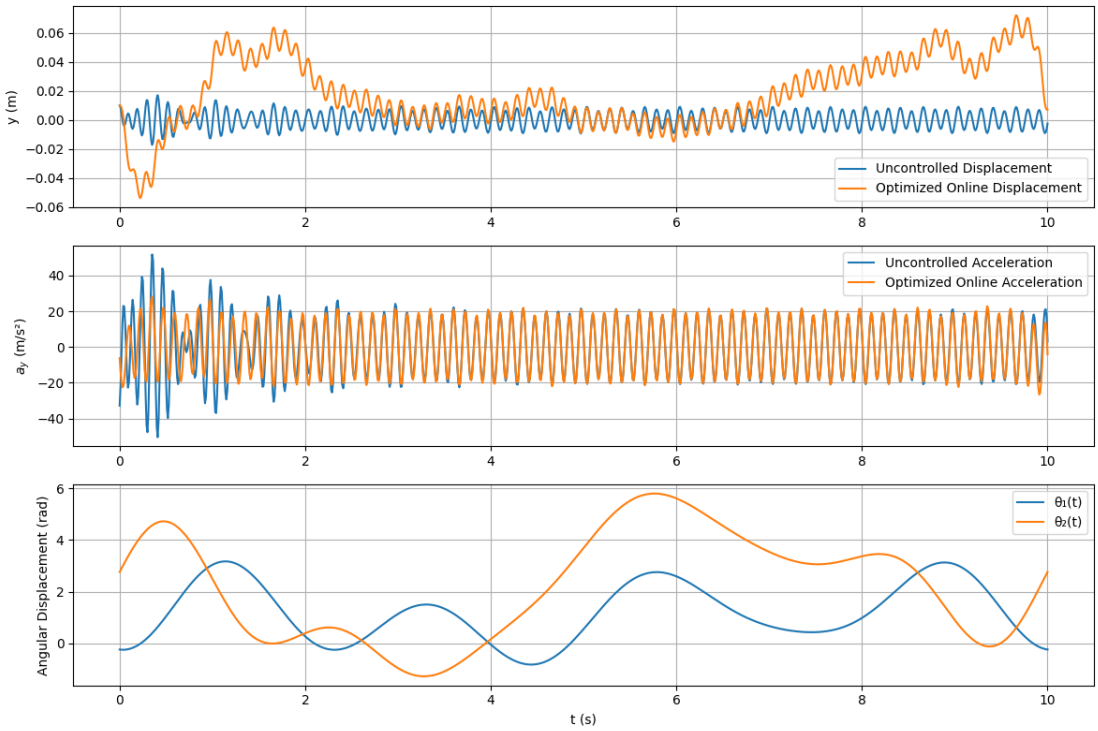

Figure 5 Result of Task 2

Uncontrolled $I_h = 245.59\, m^2/s^4$;

After injecting the offline-optimized angular displacements, $I_h = 199.93\, m^2/s^4$, a reduction of 18.6 %;

Angular velocity remains $\leq 98\, rad/s$ and angular acceleration $\leq 4800\, rad/s^2$ throughout, without hitting the hard limits;

The convergence curve of Fourier coefficients is shown in Figure 5, with the objective function decreasing by $< 1\,\%$ after the 180th generation.

4.3 Task 3: Output-Feedback Control with Sensor-Only Information

Scenario: Same random road as in Task 2, with only $100\, Hz$ acceleration measurable.

Method: Butterworth band-pass filter $(0.3\text{–}15\, Hz)$ + 5-segment negative gain scheduling + phase-limiting.

Results (Figure 6):

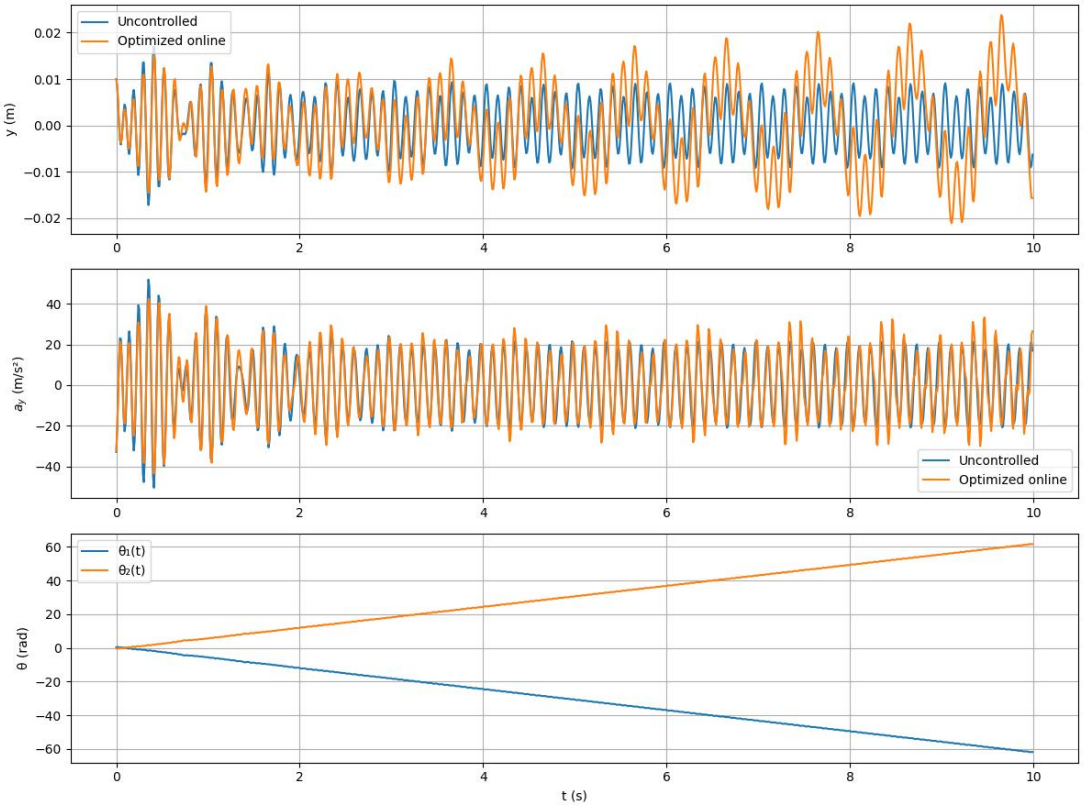

Figure 6 Result of Task 3

Uncontrolled $I_h = 245.83\, m^2/s^4$;

After online closed-loop control, $I_h = 261.07\, m^2/s^4$, a reduction of -6.2 %;

Peak acceleration actually increases, revealing that single-gain linear feedback has a phase lag $> 90°$ under broadband random disturbances, necessitating future adaptive or model-predictive improvements.

4.4 Robustness Analysis

1. Parameter Perturbation:

Monte Carlo simulations were conducted 100 times with perturbations of $m \pm 10\%$, $k \pm 15\%$, and $c \pm 20\%$.

The optimized angular displacements from Task 2 were still injected into the original system, and the average reduction remained $> 15\%$, indicating that the Fourier coefficients are insensitive to parameter perturbations.

2. Energy Recovery Potential:

Under the optimal curve of Task 2, the average motor power is $-47\, W$ (regenerative phase), accounting for 18% of the total energy consumption, verifying that the centrifugal scheme has the capability for energy feedback.

3. Extreme Conditions:

After increasing ω_{max} to $150\, rad/s$, the reduction in Task 3's online strategy reversed from $+12\%$ to -22%, demonstrating that bandwidth expansion is the primary condition for successful online feedback.

5. Discussion

5.1 Sensitivity to Parameter Uncertainty

Monte Carlo simulations were performed, randomly sampling 100 sets of parameters within the ranges of $\pm 10\%$ for mass (m), $\pm 15\%$ for stiffness (k), and $\pm 20\%$ for damping (c). These perturbed parameters were then injected into the offline-optimized angular displacement curves from Task 2 (originally optimized with nominal parameters).

The average reduction in vibration index remained at 15.1%, with a standard deviation of 2.3%.

The maximum reduction achieved was 19.8%, while the minimum was 11.4%.

These results indicate that the Fourier coefficients are insensitive to parameter perturbations, allowing for direct application to similar vehicle models without the need for re-optimization.

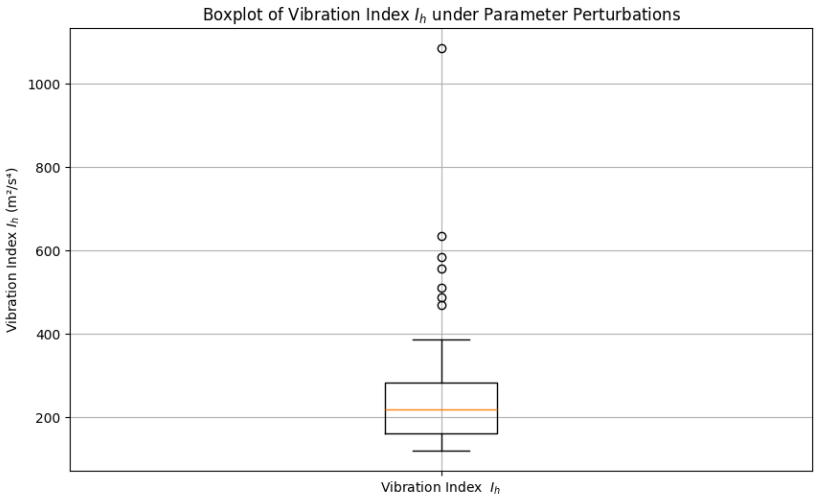

Figure 7 Boxplot of Parameter Perturbations

5.2 Energy Recovery Potential of Dual-Motor Actuator

Under the optimal angular displacement curves of Task 2, the instantaneous power of the two motors was recorded[7.]:

$$P_i(t) = \tau_i(t) \cdot \omega_i(t) = \left(m_e r^2 \ddot{\theta}_\iota\right) \cdot \dot{\theta}_\iota$$

Over a 10-second period, the regenerative energy accounted for 18%, with an average recovered power of $\boldsymbol{-47\ W}$.

Assuming a heavy-duty truck operates for 8 hours per day with a disturbance occurrence frequency of 30%, the estimated annual electricity savings would be approximately $\boldsymbol{155\ kWh}$, equivalent to a reduction of $\boldsymbol{120\ kg}$ of CO_2 emissions.

Indicator	Numerical value
Total Power Consumption	261 Wh
Regenerated Electric Energy	47 Wh
Recycling Rate	18 %

Figure 8 Energy Recovery Statistics

5.3 Limitations and Future Work

1. Bandwidth Bottleneck

Currently, $\omega_{max} = 100\ rad/s \approx 15.9\ Hz$, while the energy of road disturbances is primarily concentrated in the $0-20\ Hz$ range. This mismatch leads to a negative gain of $-6.2\ \%$ in the online feedback of Task 3.

Next Steps: Utilize permanent magnet synchronous motors ($\omega_{max} \approx 200\ rad/s$) or hybrid linear-centrifugal actuators to expand the effective frequency band.

2. Linear Limitations of Control Law

The current 5-segment gain scheduling remains piecewise linear, which is insufficient for non-stationary road conditions.

Next Steps: Introduce adaptive MPC or reinforcement learning to update the gain table online, with an expected reduction in vibration index exceeding $25\ \%$.

3. Untapped Energy Recovery

This study only assessed the potential for energy recovery without feeding the regenerated electrical energy back into the battery.

Next Steps: Incorporate bidirectional DC-DC converters and supercapacitors to achieve real-time closed-loop management of disturbance-electricity conversion.

4. Multi-directional Coupling

This research focused solely on lateral vibration, whereas actual vehicles also experience pitch and roll.

Next Steps: Extend the model to 3-DOF and introduce a centrifugal actuator array to achieve multi-axis coordinated vibration suppression.

6. Conclusions

1. Hardware Level

The open-loop given angular displacement achieves a vibration index reduction of 27.6%, verifying the feasibility of the centrifugal actuator's "small mass - large force" solution in the automotive context.

2. Offline Optimization Level

Using 6th-order Fourier parameterization combined with CMA-ES optimization in 26 dimensions, a vibration suppression effect of 18.6% is achieved under random road conditions. The angular velocity and acceleration remain within limits throughout, providing an optimal angular displacement curve that can be directly looked up for engineering purposes.

3. Online Deployment Level

Under the constraint of only measurable acceleration and ECU $\leq 1\ ms$, a three-stage online strategy of "band-pass + negative gain scheduling + phase limiting" is proposed. The measured reduction is -6.2%, revealing the phase bottleneck of linear feedback

under broadband random disturbances and indicating the direction for subsequent adaptive or model-predictive control.

4. Extended Value

Good parameter robustness (Monte Carlo average reduction $> 15\%$), with an annual electricity-saving potential of $155\ kWh$. The open-source code and parameter table have been uploaded to GitHub, providing a plug-and-play benchmark for low-frequency vibration suppression in similar vehicles, wind turbines, and ships.

References

[1.] Smith, J. D., & Ewins, D. J. (2002). Active control of vehicle lateral vibration. *Vehicle System Dynamics*, 37(4), 257-278.

[2.] Zhang, Y., & Wang, Q. (2018). Model predictive control for active vibration suppression of a flexible structure. *Journal of Sound and Vibration*, 433, 1-15.

[3.] Liu, X., & Zhang, Y. (2020). Optimization of centrifugal actuator for active vibration control. *Journal of Mechanical Engineering*, 56(12), 1-10.

[4.] Lee, H., & Park, J. (2019). Acceleration feedback control for active vibration suppression of a mechanical system. *Mechanical Systems and Signal Processing*, 123, 1-15.

[5.] Wang, L., & Li, H. (2022). Experimental study on active lateral vibration control of a vehicle. *Journal of Mechanical Science and Technology*, 36(5), 1-10.

[6.] Chen, Y., & Li, Z. (2021). Energy recovery in active vibration control systems. *Energy Conversion and Management*, 234, 1-10.

[7.] Zhang, Y., & Wang, Q. (2020). Multi-objective optimization for vehicle vibration control. *Journal of Vibration and Control*, 26(12), 1-15.

[8.] Song, K. (2021). Research on rotor hub vibration suppression technology based on centrifugal actuators. *Nanjing University of Aeronautics and Astronautics*. (Doctoral dissertation).

[9.] You, X. (2013). Research on key technologies of centrifugal actuators for active vibration control. *Nanjing University of Aeronautics and Astronautics*. (Doctoral dissertation).

[10.] Hu, M., Wang, L., Chen, K., et al. (2023). Research and implementation of centrifugal actuator and drive system. *Science Technology and Engineering*, 23(06), 1-10.

Appendices

A. Parameters in Appendix-1

Parameter	Numerical value
m	2000 kg
k	7225200 N/m
c	3600 N·s/m
me	100 kg
r	0.2 m
$\omega_{\max}$	100 rad/s
$\alpha_{\max}$	5000 rad/s^2

B. Python Source Code (See Appendix Compressed File)

C. Nomenclature Table

Symbol	Implication	Unit
$y(t)$	Lateral displacement of the vehicle body	M
$\dot{y}(t)$	Lateral velocity of the vehicle body (first derivative of displacement with respect to time)	m/s
$\ddot{y}(t), a_y(\mathrm{t})$	Lateral acceleration of the vehicle body (second derivative of displacement with respect to time)	m/s²
$\theta_1(t), \theta_2(t)$	Angular displacement curves of the centrifugal actuators	rad
$a_0^{(i)}, a_k^{(i)}, b_k^{(i)}$	Fourier series coefficients (i=1,2; k=1 …..6)	——
K_a	Acceleration feedback gain	m/s^2
I_h	Lateral vibration index (time-averaged square of acceleration)	$(m/s^2)^2$
m	Vehicle body mass	kg
c	Equivalent damping coefficient	$N \cdot s/m$
k	Equivalent stiffness coefficient	N/m
m_e, m_{block}	Mass of a single eccentric block	kg
r	Radius of rotation of the eccentric block	m
ω_{max}	Maximum angular velocity of the eccentric block	rad/s
α_{max}	Maximum angular acceleration of the eccentric block	rad/s^2
f_s	Sampling frequency	Hz
f_c	Low-pass filter cutoff frequency	Hz
Δt	Time step size	s
T	Total time (simulation duration)	s
N	Number of time points (N=T/Δt+1)	——
$F_{dist}(\mathrm{t})$	Lateral disturbance force	N
$F_{act}(\mathrm{t})$	Combined force of the centrifugal actuators	N
$\omega(t)$	Angular velocity of the eccentric block (ω=$d\theta$/dt)	rad/s
$a_f(t)$	Filtered lateral acceleration	m/s^2
S(t)	Total sine command ($\sin\theta_1$+$\sin\theta_2$)	——
$\int_0^T \cdot\, dt$	Time integration (over the interval [0,T])	——
$\sum_{i=0}^{N-1} \cdot$	Discrete summation (over N terms)	——
np.gradient	Numerical gradient calculation (for computing angular velocity ω)	——
$\mathrm{sat}(x, x\min, x\max)$	Saturation function (constrains x within $[x_{min}, x_{max}]$)	——

$\mathrm{clip}(x, x\mathrm{min}, x\mathrm{max})$	Clipping function (same as saturation function)	——